Proceedings of the Sixth International ASME Conference on Nanochannels, Microchannels and Minichannels
ICNMM2008
June 23-25, 2008, Darmstadt, Germany

ICNMM2008-62239

ELECTROKINETIC ACTUATION OF LOW CONDUCTIVITY DIELECTRIC LIQUIDS

Rohan Raghavan [1] rohan.raghavan@eng.monash.edu.au
Jiaxing Qin [1] jiaxing.qin@eng.monash.edu.au
Leslie Y. Yeo [1] leslie.yeo@eng.monash.edu.au
James R. Friend [1] james.friend@eng.monash.edu.au
Kenjiro Takemura [2] takemura@mech.keio.ac.jp
Shinichi Yokota [3] syokota@pi.titech.ac.jp
Kazuya Edamura [4] edamura@a2.mbn.or.jp

ABSTRACT

There has been some amount of confusion over the origin of electrohydrodynamic phenomena responsible for the actuation of dielectric fluids in the presence of an electric field. Previous studies have accounted for the possibility of conduction pumping, ion drag pumping and induction pumping as driving mechanisms but have ignored the possibility of Maxwell (electric) pressure driven flow. Until recently, this mechanism has been poorly understood and as a result has often been overlooked. This paper demonstrates how a Maxwell pressure gradient can induce flow in dielectric liquids in the presence of a non-uniform field. We derive, from first principles using lubrication theory, an expression for the flow velocity which exhibits a quadratic dependence on the applied voltage and also proportionality to the ratio of the permittivity and viscosity. The theoretical predictions are supported by experimental results. Although we have examined the phenomenon for a particular class of dielectric liquids, it is believed that this mechanism could well be responsible for the actuation of other low conductivity dielectric fluids previously attributed to conduction or ion drag pumping. In any case, we discuss ways to identify the dominant mechanism by comparing the salient features for a given type of flow.

1.0 NOMENCLATURE

$\vec{F}_e$	Electric body force density (N/m^3)
q_s	Net electric surface charge density (C/m^2)
q_v	Net electric volume charge density (C/m^3)
A	Cross sectional area (m^2)
$\vec{E}$	Electric field (V/m)
ε	Electric permittivity (F/m)
ρ	Fluid density (kg/m^3)
b	Charge mobility (m^2/V.s)
v	Charge velocity (m/s)
u	Fluid velocity (m/s)
j	Current density(A/m^2)
p	Hydrodynamic pressure (Pa)
V	Voltage (V)
I	Current (A)
μ	Dynamic viscosity (Pa.s)
σ	Electrical conductivity (S/m)
h	Height (m)
x	Distance along channel (m)
L	Channel length (m)

Subscripts:

g	Gas phase
l	Liquid phase
n	Normal component
t	Tangential component

2.0 INTRODUCTION

Dielectric fluids are commonly employed in microfluidic devices; however, their low conductivities preclude the use of electroosmosis as an actuation mechanism. As a result, research over the last few decades has focussed on the development of electrohydrodynamic (EHD) microfluidic pumps in order to actuate these fluids. The absence of mechanical parts, lightweight construction, reliability, low power consumption and the ability to generate considerable flow velocities have made EHD the obvious choice of actuation in heat transfer and micropumping devices involving dielectric fluids [1].

EHD flow is induced when a dielectric fluid is subjected to a non-uniform electric field. To date, four proposed mechanisms have been put forth in order to explain the observed EHD phenomena. These mechanisms are ion injection, conduction pumping, Maxwell (electric) pressure gradients and induction pumping. While the first two mechanisms rely on the presence of space charge in the fluid, the remaining two depend on the polarization induced within the dielectric liquid. Nevertheless, there seems to be considerable confusion in the literature over the specific conditions that promote each of the mechanisms in discussion. In this paper we aim to explain the differences between each mechanism and verify through theory and experiments that the

[1] Micro/Nanophysics Research Laboratory, Monash University, Clayton, VIC 3800, Australia
[2] Keio University, Japan
[3] Precision and Intelligence Laboratory, Tokyo Institute of Technology, Japan
[4] New Technology Management Co. Ltd., Tokyo, Japan

Maxwell pressure gradient driven flow is responsible for the EHD phenomena in at least a particular class of dielectric liquids.

The electric body force density acting on a liquid is described by the Korteweg-Helmholtz equation:

$$\vec{F}_e = q_v \vec{E} - \frac{1}{2}\vec{E}^2 \nabla \varepsilon + \frac{1}{2}\nabla\left[\rho \vec{E}^2 \left(\frac{\partial \varepsilon}{\partial \rho}\right)_T\right]. \quad (1)$$

One can infer the presence of three different components of the force density which can give rise to fluid flow [2]. In (1), the first term accounts for the Coulombic force exerted on free charges in the presence of an electric field. The second term refers to a dielectric force which is induced in the presence of a permittivity gradient. A local change in permittivity may be experienced in the presence of a liquid/vapour or liquid/liquid interface, or due to the existence of non-isothermal conditions in a single phase liquid. The third term in the force density equation deals with the electrostriction force which occurs in compressible media. Hence a force upon a weakly conducting, incompressible dielectric fluid under isothermal conditions can only be generated if space charges are introduced or if there exists a jump in permittivity across the normal field. These two mechanisms therefore form the basis of all the dielectric actuation principles we shall be discussing.

The remainder of this section will provide a brief review on the three prevalent mechanisms, namely, ion injection, conduction pumping and induction pumping. In Section 3, we then discuss and develop the theory for Maxwell pressure gradient driven flow. This is followed by a description of the experiments carried out to elucidate the governing EHD mechanism for a particular class of fluids. Our focus here is primarily on a group of fluids known as Electro-Conjugate Fluids (ECFs) that have recently been used in several EHD applications [3-5]. Our motivation behind the choice of these fluids was the lack of understanding of the underlying actuation mechanism. From a generic viewpoint, these fluids may be treated as typical low conductivity homogeneous dielectric liquids for which either one of the four mechanisms may dominate in creating flow under an applied electric field. The results are discussed in Section 5, and finally, the conclusions are summarised in Section 6.

2.1 Ion Injection

Ion injection pumping, also known as ion-drag pumping, involves the direct injection of charges into an insulating dielectric fluid by a corona source [6]. The injected unipolar charges migrate to the low field region and in the process collide with the molecules of the insulating fluid. This transfer of momentum gives rise to bulk fluid flow. Pumping with this mechanism was first proposed by Stuetzer in the late 1950s and has since been widely researched and implemented in numerous micro-cooling and micro-pumping devices [7-9]. Ion injection is apt for situations that demand high pressure heads and where the degradation of the working fluid can be ignored. A disadvantage however is the large field strengths commensurate with threshold ionization voltages, typically 100 kV/cm, that are required to drive the mechanism [10].

A typical ion injection or ion-drag pump utilises a sharp needle-like emitter electrode and a perforated or hollow collector electrode. Corona discharge at the tip of the emitter then directly injects charges into the working fluid. These charges subsequently experience a Coulombic force as a result of the electric field. Consequently, the motion of these charges away from the high field region induces bulk flow in the insulating fluid in the same direction. Figure 1 illustrates a generic ion-drag pump configuration.

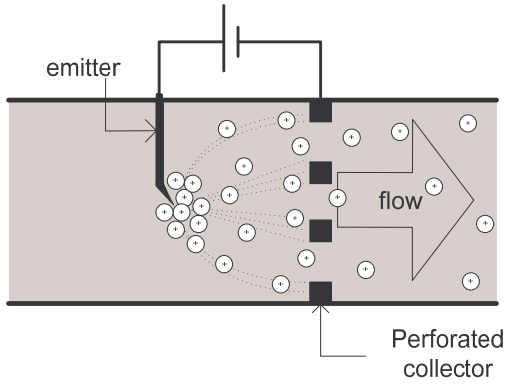

Figure 1: Schematic of the ion injection pumping mechanism.

The drift velocity, v, of an ion in an electric field is given by the

$$\vec{v} = b\vec{E}, \quad (2)$$

where b refers to the ion mobility in the fluid. Taking bulk flow into account allows us to rewrite (2) as

$$\vec{v} = b\vec{E} + \vec{u}, \quad (3)$$

where $\vec{u}$ refers to the fluid velocity with respect to the electrode. Hence, the expression for the current density, j, in an ion drag pump becomes

$$j = (b\vec{E} + u)q_v. \quad (4)$$

Neglecting inertial and viscous forces, the pressure gradient developed can be related to the Coulombic force on an ion such that

$$\frac{\partial p}{\partial x} = q_v \vec{E}. \quad (5)$$

Eliminating q_v from (5) using (4) and since $j=I/A$, we obtain

$$\frac{\partial p}{\partial x} = \frac{I}{Ab}. \quad (6)$$

Integrating (6) over channel length x to x_0 gives us Chattocks relation

$$p - p_0 = \frac{I}{Ab}(x - x_0). \quad (7)$$

Using Gauss's Law and a combination (4), (5), (6) and (7) such that $I/A=q_v b\vec{E}$ results in

$$(p - p_0) = \frac{\varepsilon}{2}(\vec{E} - \vec{E}_0)^2, \quad (8)$$

when integrated over the channel length x [11]. From (2) it is also evident that that the fluid velocity, imparted by the ions, also scales linearly to the applied voltage.

An ion-drag pump can function in two modes: field ionisation and field emission. The former requires a setup similar to that shown in Figure 1, i.e. with the high voltage end connected to the emitter. In this case, the high field strength causes the electrons to be transferred from the surrounding fluid to the electrode creating a collection of positively charged ions that are repelled away from the electrode. Field emission occurs

with electrons being injected into the liquid when a high voltage electrode of negative polarity is connected to the emitter [12]. In both cases, ion-drag pumping is characterised by bulk flow towards the low field region, large currents and the existence of a threshold field strength, beyond which fluid actuation commences [10].

2.2 Conduction Pumping

As with ion-drag pumping, bulk flow due to this mechanism also requires the presence of space charge in the fluid. However, the two rely on markedly different methods of charge generation. Onsager showed that the increase in the ion dissociation rate of weak electrolytes (low conductivity dielectrics) in the presence of an electric field is proportional to the field strength and inversely proportional to the dielectric constant of the fluid [13]. Reiss further adapted this theory to attribute charge generation in dielectrics to the dissociation of trace polar impurities in the fluids and in some cases, the molecules of the dielectric themselves [14]. More recently, Yagoobi et al. conducted several theoretical and experimental studies on the effectiveness of this phenomenon as a pumping mechanism [1, 10, 15].

Conduction pumping of low conductivity dielectrics involves the formation of bipolar charges by the Faradaic dissociation of either polar impurities or the dielectric molecules or a combination of both [16]. As in the case of ion-drag pumping, electromigration of these charges then induces bulk flow in the liquid. In Figure 2, a pressure gradient is established due to the imbalance in the forces on the cations and anions produced. These migrating ions settle at the corresponding electrodes to create heterocharge layers with thicknesses proportional to the permittivity of the working fluid and the applied voltage [15].

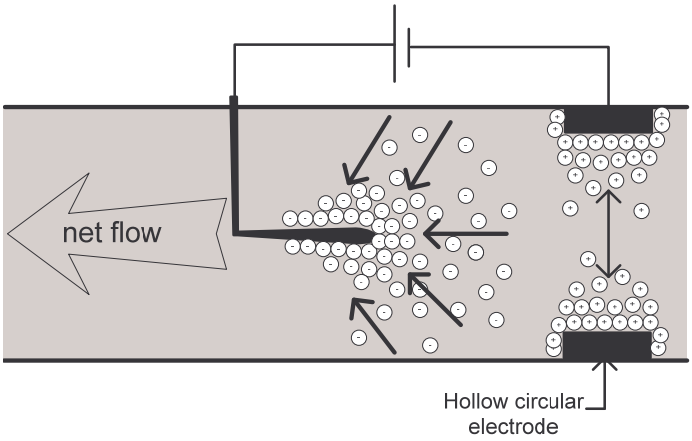

Figure 2: Schematic of the conduction pumping mechanism.

Like the ion-drag pump, the operation of a conduction pump is governed by equations similar to (2-8). Consequently fluid velocity in a conduction pump also scales linearly with the applied voltage whilst the pressure scales to its square. Since bipolar conduction occurs in a conduction pump, a net flow can arise only if the electrode configuration is asymmetrical or if a non-uniform field is established within the fluid. Conduction pumping is characterised by fluid flow towards the high field region and by the existence of a field strength threshold of 1 kV/cm for fluid actuation.

At sufficiently high field strengths, typically greater than 1 kV/cm, the energy required to break the hydrogen bonds in the dielectric molecules is lowered, resulting in the ionization of the fluid. Regardless of whether it is the dissociation of impurities or the dielectric molecules, the formation of heterocharge layers would eventually cause charge equilibrium, where the liquid around the electrodes would be shielded from the electric field by the charge layers. In a DC driven pump, this would prevent further ionization and allow the mechanism to operate only over short transients. However, if AC fields are employed, non-equilibrium field-induced charging effects will prevent the formation of heterocharge layers and permit the pumping to continue. It is therefore doubtful that continuous pumping can be achieved by a DC-induced conduction pumping mechanism.

2.3 Induction Pumping

EHD induction pumps were first suggested by Melcher [17] as a means of actuating insulating fluids without having the electrodes physically in contact with them. This mechanism relies on the induction of surface charges in a dielectric owing to a conductivity and/or permittivity gradient across an interface. Although most induction pumps would require the presence of an interface between two media of different electrical properties, thermal gradients in a single phase fluid have also been exploited to create a discontinuity in conductivity [2, 18].

Since electric currents in induction pumping are generally low, the interference due to magnetic induction would also be negligible, leading to the assumption of an irrotational field [17]. As a result, the following interfacial boundary conditions in which the tangential field is assumed to be continuous across the interface and the jump in the normal component of the electric displacement across the surface is given by the net surface charge, q_s, apply:

$$\left[\vec{E}_t\right]_l^g = 0 \ , \tag{9}$$

$$\left[\varepsilon\vec{E}_n\right]_l^g = q_s \ . \tag{10}$$

Conservation of momentum requires

$$\rho\left(\frac{\partial u}{\partial t} + \vec{u}\cdot\nabla\vec{u}\right) = \nabla\cdot\mathbf{T} \ , \tag{11}$$

where $\nabla\cdot\mathbf{T}$ represents the total stress tensor given by

$$\nabla\cdot\mathbf{T} = -\nabla p + \nabla\cdot\mathbf{T}_V + \nabla\cdot\mathbf{T}_{\mathrm{m}} \ , \tag{12}$$

where

$$\nabla\cdot\mathbf{T}_V = \propto\left[\nabla\vec{u} + \nabla\vec{u}^T\right]. \tag{13}$$

In (12), T_v is the viscous stress and ∇p accounts for the pressure gradient due to external sources. $\mathbf{T}_{\mathrm{m}}$ is the Maxwell stress tensor which is given by [19]

$$\mathbf{T}_m = \varepsilon\vec{E}\vec{E} + \frac{1}{2}\varepsilon(\vec{E}\cdot\vec{E})\mathbf{I} \ , \tag{14}$$

where $\mathbf{I}$ is the identity tensor. The jump in the normal and tangential components of this tensor across the interface is then

$$P_{Mn} = n\cdot\mathbf{T}_m\cdot n = \frac{1}{2}\left[\varepsilon\left(\vec{E}_n\right)^2 - \varepsilon\left(\vec{E}_t\right)^2\right]_l^g \ , \tag{15}$$

$$P_{Mt} = n\cdot\mathbf{T}_m\cdot t_l = \left[\varepsilon\vec{E}_n\right]_l^g\left(\vec{E}_t\right) = q_s\left(\vec{E}_t\right) \ , \tag{16}$$

where $\vec{n}$ and $\vec{t}$ are the unit normal and tangential vectors respectively. The square parenthesis indicates a jump in the inner quantity across the interface, evaluated by subtracting the quantity for the liquid phase (*l*) from that in the gas (*g*).

From (16), it can be seen that the combination of induced charge and the tangential field at the interface gives rise to interfacial tangential shear that drags the fluid along. Balancing the viscous drag at the interface with this tangential shear force and the no-slip condition at the contact surface allows for the derivation of the steady state velocity that reveals a quadratic dependence on the applied voltage in the pump as confirmed by Melcher and Crowley et al [17, 18].

It can be seen from (10) and (16) that the length scale over which the fluid is driven is commensurate with that across which the interfacial charge and tangential field is spatially distributed. To drive continuous fluid motion across a significant length, it is therefore necessary to have sequential electrodes along the fluid interface, driven separately to form an electric field that appears to move along the interface setting up a continuous distribution of interfacial charge and tangential fields. Motion arises due the lag between the travelling wave and induced charges. Hence, induction pumps are also known as travelling wave pumps and have the ability to operate in two modes – attraction and repulsion as shown in Figures 3a and 3b, respectively. The optimal velocity of this field can be calculated using the electrode spacing (*the wavelength*) and the inverse of the relaxation time of the more conducting medium (*the frequency*). At velocities greater than this optimal value, there is insufficient time to induce charge before the field reverses; at velocities below the optimum, the pump is inefficient as there is insufficient charging.

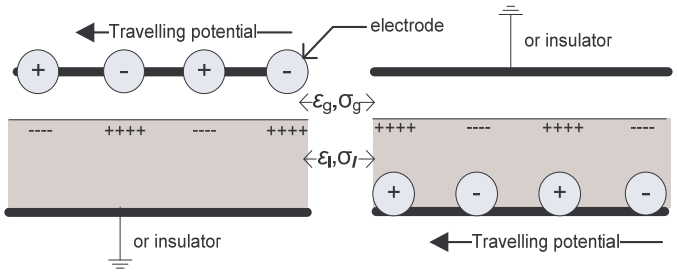

(a) Attraction pump **(b) Repulsion pump**

Figure 3: Travelling wave induction pumping.

In the attraction pump, the charges that relax at the surface are of opposite polarity to the electrode. However, in the repulsion pump, where the more conductive medium is in contact with the electrodes, the surface charges induced are of the same polarity as the adjacent electrodes. An attraction pump moves the interfacial charge layer in the direction of the field and exhibits a fluid velocity that is only limited by the velocity of the potential wave. In the repulsion pump however, fluid can flow in either direction as charges may be pumped in front of the travelling wave or behind it [18]. A highly conductive fluid, in which charge relaxation is instantaneous, does not support induction pumping. Similarly if conductivity is too small, no charges relax to the surface and the shearing effect is negligible [17]. Hence, an important point to note is that induction pumping is not suitable for dielectrics of low conductivity (< 10^{-8} S/m) as they are not conducive to surface charge.

3.0 MAXWELL PRESSURE GRADIENT FLOW

Unlike induction pumping, fluid flow due to Maxwell (electric) pressure gradients can be induced in a dielectric despite the absence of free surface charge. In situations where low conductivity leads to negligible surface charge at the interface, (10) becomes

$$\left[\varepsilon \vec{E}_n\right]_l^g \approx 0\,. \tag{17}$$

The tangential component of the Maxwell stress tensor in (16) then becomes negligible. Maxwell pressure gradient driven bulk flow arises due to the normal component of the Maxwell stress tensor given in (15). Either the normal field or the tangential field, whichever is present or dominant, or both, may give rise to the Maxwell pressure component, $\mathbf{T}_m$, that appears in (12), which can then be seen to cause flow. It is important to note that this mechanism does not necessarily have to arise through interfacial stresses. It can be better understood through the illustration provided in Figure 4 wherein the non-uniform electric field produced by the pin-plate electrode configuration gives rise to a Maxwell pressure gradient which drives the flow. At a micro scale, the vertical length represented by the liquid film or channel height *h* is usually several orders of magnitude smaller than the channel length *L*. In these small aspect ratio ($\delta \equiv h/L << 1$) flows, the gradient in the electric field in the normal direction is usually much larger than that in the tangential direction and as such, the latter can be neglected. For incompressible fluid flowing through a channel of rectangular geometry (*see* Figure 4), it then follows, assuming that the effects of curvature at the free surface are negligible, that (11) together with (12) and (14) reduce to

$$\propto \frac{\partial^2 u}{\partial y^2} = \frac{\varepsilon}{2}\frac{\partial}{\partial x}\vec{E}_n^{\,2} + \frac{\partial p}{\partial x}\,, \tag{18}$$

From [20] we can approximate the normal electric field to decay as 1/*r*, where *r* is the distance between the tip of the electrode and the point along the ground electrode. Thus,

$$\vec{E}_n = \frac{V}{\sqrt{x^2 + d^2}}\,. \tag{19}$$

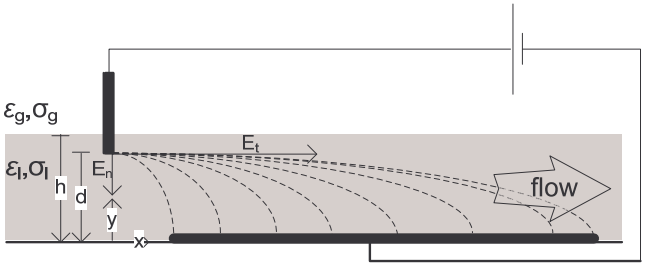

Figure 4: Maxwell pressure gradient driven flow

To render the problem dimensionless, we employ the following transformations:

$$u \to \tilde{u}\,U_0; \quad V \to \tilde{V}\,V_0; \quad x \to \tilde{x}\,L; \quad y \to \tilde{y}\,H$$

where $U_0 = \dfrac{\varepsilon V_0^2}{2\propto L}$ is the characteristic velocity obtained through an electroviscous scaling that balances the dominant viscous and Maxwell forces. In the absence of an externally imposed pressure gradient $\partial p/\partial x$, (18) may be rewritten as

$$\frac{U_0}{H^2}\frac{\partial^2 \tilde{u}}{\partial \tilde{y}^2} = \frac{\varepsilon V_0^2}{\propto L^3}\frac{\partial}{\partial \tilde{x}}\left(\frac{\tilde{V}^2}{\tilde{x}^2 + \gamma \tilde{d}^2}\right), \quad (20)$$

where $\gamma = H^2/L^2 << 1$. We now integrate (20) with the following no-slip and shear free boundary conditions at the substrate and free surface, respectively:

$$\tilde{u} = 0 \text{ at } \tilde{y} = 0, \quad (21)$$

and

$$\propto \frac{\partial \tilde{u}}{\partial \tilde{y}} = 0 \text{ at } \tilde{y} = \tilde{h}. \quad (22)$$

This results in the following velocity profile:

$$\tilde{u} = \frac{1}{3}\frac{\varepsilon V_0^2 \tilde{V}^2}{\propto \tilde{x}^3 L^3}\frac{H^2 \tilde{h}^2}{U_0}. \quad (23)$$

Substituting U_0 and integrating this expression over the channel height h and length L results in the following average cross sectional velocity

$$\langle \tilde{u} \rangle = \frac{1}{75}\tilde{V}^2. \quad (24)$$

(24) indicates a quadratic dependence between the fluid velocity and the applied voltage. The redimensionalization of (24) results in

$$\langle u \rangle = \frac{\varepsilon}{150 \propto x} V^2 \quad (25)$$

which shows how the average flow velocity across the channel takes into account the properties of the working fluid.

4.0 EXPERIMENT

Figure 5 shows the isometric and lateral views of the experimental setup. The body of the rig was machined out of transparent perspex in order to observe the motion of the fluid through its base. A 5 mm square open channel was machined through the centre of the body in a manner that allowed recirculation of the fluid when pumped through it. The bottom surfaces of these channels were constructed out of glass coated with Indium Tin Oxide (ITO) with a dual purpose of permitting visualisation and functioning as the conducting ground electrode. A vertical titanium pin was mounted at the opening of the channel at a height d above the ITO base to function as the positive electrode as shown in Figure 4. A non-uniform electric field is then generated across the entire channel length L when a voltage is applied to the pin electrode.

Isometric View

Lateral View

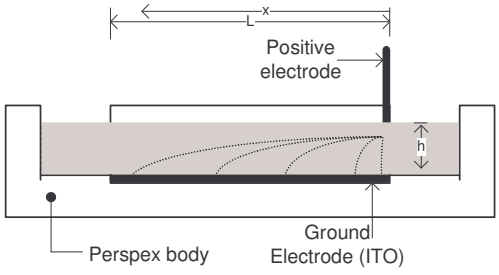

Figure 5: Experimental setup

In order to obtain a unidirectional flow, the position of the pin is very important. Unlike electroosmotic pumps where electrodes are placed at both ends of the fluidic channel, the pin electrode for Maxwell pressure gradient-driven pumps must be placed at the opening of the channel in order to establish the required Maxwell pressure gradient and hence promote pumping along the length of the channel. If the pin is placed in the middle of the channel, no net flow will result as pressure gradients are generated towards both ends of the channel resulting in bidirectional flow away from the centre. In order to prevent the occurrence of ion injection, the pin was coated with Teflon® and was also devoid of a sharp edge at its tip. Care was taken to immerse the electrode tip slightly beneath the surface of the liquid to ensure the existence of an electric field in the liquid phase. A 1 mm gap d was maintained between the tip of the positive electrode and the ground electrode's surface.

The theoretical prediction in (24) was verified through high speed video microscopy using an inverted fluorescence microscope (Olympus IX71) connected to a high speed camera capable of imaging at up to 2000 frames/s by seeding the flow field with 8 ∝m polystyrene particles from Duke Scientific (Cat. No. 36-3). The velocity of the fluid for different applied voltages (0 to 5000 V) was then calculated from the captured particle trajectories with the use of particle tracking software that accompanied a Micro Particle Image Velocimetry System (Dantec Dynamics).

Three different weakly conducting dielectric fluids were used to corroborate theory with experiments. The choice of these fluids was deliberate. Recently, the DC electric-field pumping of a class of low conductivity dielectric fluids, the so-called Electro-Conjugate Fluids (ECFs) [4, 5] was demonstrated. However, the mechanism by which these fluids were actuated was unknown. It is therefore the intention of this paper to provide evidence that the flow of these fluids arises due to the existence of Maxwell pressure gradients when the non-uniform electric field is applied. The fluid properties of the specific dielectric fluids used in this study are detailed in the table below [21]. The working fluid and the particles were replaced after each experiment to avoid contamination and the coagulation of particles.

Table 1: Working fluid properties

Name	Conductivity (S/m)	Viscosity (Pa.s)	Permittivity (F/m)
Dibutyl Decanedioate (DBD) $C_{18}H_{34}O_4$	4.70×10^{-10}	7.00×10^{-3}	4.54×10^{-11}
Linalyl Acetate $C_{12}H_{20}O_2$	1.82×10^{-9}	1.30×10^{-3}	4.46×10^{-11}
Dibutyl Adipate $C_{14}H_{26}O_4$	3.01×10^{-9}	3.5×10^{-3}	4.6×10^{-11}

Since dielectric particles within a dielectric medium suffer from dielectrophoresis (DEP) [22], the particle DEP velocities u_{DEP} have to be accounted for when determining the true flow velocity u from the apparent (*observed*) particle velocity u_{app}. In particular, polystyrene particles exhibit positive DEP in the presence of a low frequency *(here we employ DC)* electric field

[23, 24]. Unlike Maxwell pressure gradient driven flow, positive DEP drives particle flow *towards* the high field region. Thus,

$$u = u_{app} + u_{DEP}; \tag{26}$$

where

$$u_{DEP} = \frac{\varepsilon_l r^2 \,\mathrm{Re}[f_{cm}]V^2}{18\propto d^3}, \tag{27}$$

in which ε_l is the liquid permittivity and r the particle diameter, and

$$f_{cm} = \frac{\sigma_p - \sigma_l}{\sigma_p + 2\sigma_l}, \tag{28}$$

where σ is the conductivity. The subscripts p and l denote the particle and liquid medium respectively. Re[f_{cm}] therefore corresponds to the real part of the Clausius Mossotti factor at the low frequency asymptote since a DC field is employed. We note that u_{DEP} is small, typically in the order of 10^{-7} to 10^{-3} m/s.

5.0 RESULTS AND DISCUSSIONS

The experiments revealed the generation of a unidirectional flow away from the high field region which is consistent with Maxwell pressure gradient driven flow. Moreover, Figures 6 and 7 verify the existence of a quadratic relationship between the flow velocities and the applied voltage as predicted in (25). Good agreement between the theoretical prediction (*solid lines*) and experimental data (*markers*) shown in Figure 6 further gives credence to the idea that flow is driven by a Maxwell pressure gradient. Figure 7 depicts the relationship between the obtained fluid velocities and the ratios of their permittivity and viscosity. The gradients obtained from the graphs in this figure closely match their respective theoretical values.

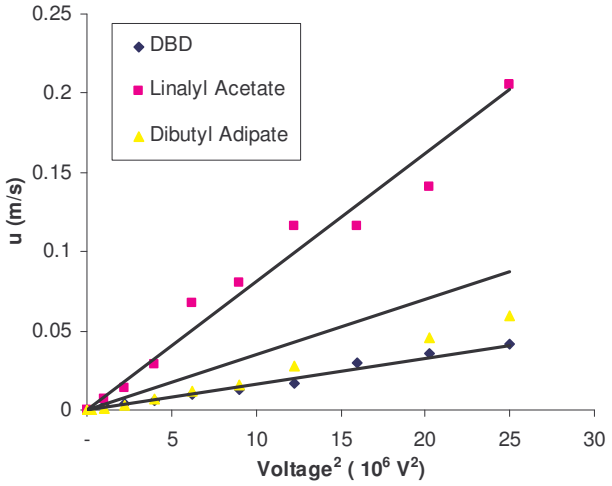

Figure 6: Plot of induced velocity as a function of the square of the voltage for the experimental and theoretical data.

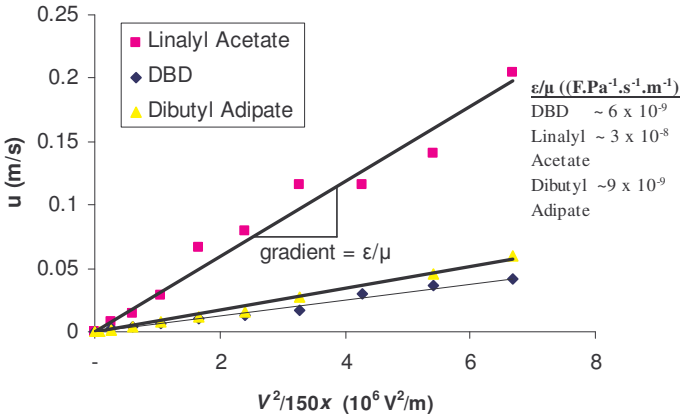

Figure 7: Dependence of the velocity on the ratio of the liquid's permittivity to its viscosity.

In Figure 8, the experimental data in Figures 6 and 7 is collapsed using the electroviscous scaling employed in (20). It can be seen that the rescaled data matches reasonably well with the universal scaling given by (24). The slight discrepancy between the theoretical prediction and the experimental data is likely to be due to the use of lubrication theory which assumes that the channel dimensions conform to those of a thin film of liquid. The small mismatch in aspect ratios between the two models might be the reason for the discrepancy. We have reason to believe that this universal scaling with the dimensionless squared voltage applies to all low conductivity dielectric fluids. Further experiments will be conducted with more fluids to verify that the Maxwell pressure gradient mechanism is the relevant dominant mechanism in the actuation of these fluids.

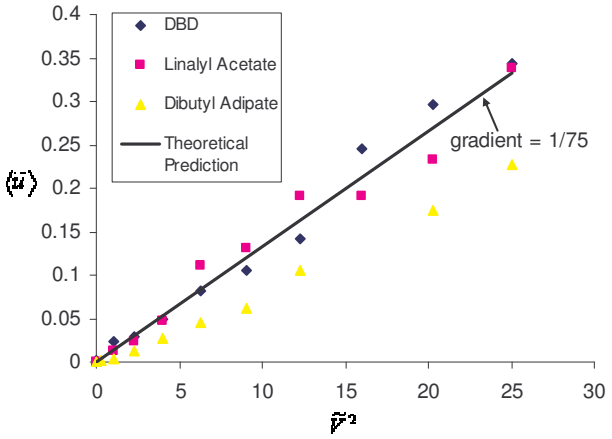

Figure 8: Collapse of the experimental data using the electroviscous velocity scaling in (24) as a function of the dimensionless voltage squared.

The non-linear relationship between the fluid velocity and voltage suggests that the ion injection and conduction pumping mechanisms are not the major contributors towards flow, at least for the low conductivity fluids used in our experiments. Furthermore, ion injection and conduction pumping stipulate that the flow only commences beyond a threshold electric field intensity of 100 kV/cm and 1 kV/cm respectively. Neither of these thresholds was reached in our experiments. Indeed, no

such threshold was observed in our experiments; we observed the flow occurring at even low field strengths.

The absence of a threshold voltage for flow as well as the quadratic velocity scaling with respect to the applied voltage makes induction pumping a possible mechanism. However, induction pumping requires the generation of a spatial distribution of charge at the interface, which is possible if the dominant field were in the gas phase and if an AC travelling wave potential were to be applied, neither of which are applicable in our case. Moreover, the use of low conductivity dielectrics suggests weak interfacial polarization, thus eliminating induction pumping as a plausible actuation mechanism. Furthermore, even if induction pumping was to occur, our setup would qualify as a repulsion pump (Figure 3b), driving flow towards the high field region around the pin electrode, which is clearly not the case. As such, we provide clear evidence that it is the existence of Maxwell pressure gradients that is the driving mechanism for the pumping of the fluids observed here. It should be noted that unlike induction pumping, the current mechanism could involve a free surface, but can also occur without one, thus allowing the channel to be closed without requiring a fluid-fluid or fluid-air interface.

6.0 CONCLUSIONS

Despite more than a decade of research, there is still considerable confusion in the literature when it comes to identifying the dominant mechanism in driving dielectric fluid flow using electric fields. Ion injection (ion drag pumping), conduction pumping, induction pumping and Maxwell pressure gradients have been proposed as potential candidates for driving the electrohydrodynamic flow of dielectric liquids. Further confusion and suspense has been created by experiments that demonstrate the pumping of a class of low conductivity dielectric fluids termed as electro-conjugate fluids [4, 5] for which the actuation mechanism has not been understood. In this paper, we briefly review the various mechanisms, and identify salient features that are associated with each mechanism in pumping fluids using electric fields, providing useful clues to help identify the mechanism behind the ECF fluid pump and other devices as well. We stress that these provide clues that help identify the dominant mechanism in play. The differentiation features are

1. The existence of a threshold electric field for the commencement of fluid flow.
2. The direction of the flow with respect to the electrodes (*towards high or low field regions*).
3. The scaling relationship between the velocity and the applied voltage.

These attributes in the context of the described mechanisms herein are summarised in Table 2. Using this information it is possible to identify the dominant mechanism responsible for an observed flow based on these differential characteristics alone.

We have chosen to examine a particular class of liquids, i.e., the electro-conjugate fluids described above, due to their recent 'discovery' and lack of knowledge about the mechanism by which flow arises under the application of an electric field. Our experiments show the existence of flow in the absence of a threshold voltage, the flow being driven from the high field region towards a low field region in which the velocity scales *quadratically* with the applied voltage. These features immediately point towards Maxwell pressure gradients as the driving mechanism. Moreover, predictions obtained from the universal scaling in (24) which was derived using the simple lubrication model, seem to agree well with the experimental data, adding credence to the proposed mechanism. Despite the simplicity of the model, the data is observed to collapse when the velocity is scaled using an electroviscous scaling, indicating the obvious balance between the viscous and Maxwell stresses. The fluid permittivity and viscosity are important flow parameters here; we note the absence of conductivity effects in the model, suggesting that ion generation gives rise to space charges and their subsequent migration under the electric field is not important. Instead, dielectric polarization induced at the surface of the electrode gives rise to a body force that is translated into bulk flow. This has largely been overlooked in previous studies. It is impractical for us at this stage to repeat the vast body of experiments that have been carried out previously. Nevertheless, we believe that if the experimental data of these studies were to be re-examined closely, it would not be surprising if Maxwell pressure gradients play a dominant role as the driving fluid actuation mechanism in at least some of the work.

Table 2: Attributes of different pumping mechanisms

Mechanism	Threshold (kV/m)	$u \propto$	Flow Direction
Ion injection (ion-drag)	10^4	V	High field to low field
Conduction	10^2	V	Low field to high field
Induction	0	V^2	Either direction
Maxwell pressure gradient	0	V^2	High field to low field

Acknowledgement

Funding for this project through the Australian Research Council Discovery Project scheme (Project Number: DP0666660) is acknowledged.

7.0 REFERENCES

1. Feng, Y. and Seyed-Yagoobi, J., *Understanding of electrohydrodynamic conduction phenomenon.* Physics of Fluids, 2004. 16(7); p. 2432–2441.
2. Melcher, J.R., ed. *Continuum Electromechanics*. 1981.
3. Takemura, K., Yokota, S. and Edamura, K. *A Micro Artificial Muscle Actuator using Electro-conjugate Fluids*. in *International Conference on Robotics and Automation*. 2005. Barcelona: IEEE; p. 532-537.
4. Otsubo, Y. and Edamura, K., *Dielectric Fluid Motors.* Applied Physics Letters, 1997. 71(3): p. 318-320.
5. Yokota, S., Kondoh, Y., Sadamoto, A., Otsubo, Y. and Edamura, K., *A Micro Motor Using Electro-conjugate Fluids (ECF) (Proposition of Stator Electrode-type (SE-type) Micro ECF Motors).* JSME International Journal Ser C, 2001. 44(3): p. 756-762.

6. Baker, E.B and Bolts, H.A., *Thermionic Emissions into Dielectric Liquids.* Physical Review, 1937. 51: p. 275.
7. Stuetzer, O.M., *Ion-Drag Pressure Generation.* Journal of Applied Physics, 1959. 30: p. 984-994.
8. Foroughi, P., Benetis, V., Ohadi, V. *Design, Testing and Optimization of a Micropump for Cryogenic Spot Cooling Applications*. in *21st Annual IEEE SEMI-THERM Symposium* 2005.
9. Darabi, J., and Wand, H., *Development of an Electrohydrodynamic Injection Micropump and its Potential Application in Pumping Fluids in Cryogenic Cooling Systems.* Journal of Microelectromechanical Systems, 2005. 14(4): p. 747-755.
10. Seyed-Yagoobi, J. and Jeong, S., *Theoretical/Numerical Study of Electrohydrodynamic Pumping Through Conduction Phenomenon.* IEEE Transactions on Industry Application, 2003. 39(2): p. 355.
11. Stuetzer, O.M., *Ion Drag Pumps.* Journal of Applied Physics, 1960. 31(1): p. 136-146.
12. Al Dini, S.A.S., *Electrohydrodynamic Induction and Conduction Pumping of Dielectric Liquid Film: Theoretical and Numerical Studies*. PhD Thesis, 2005, Texas A & M University.
13. Onsager, L., *Deviations from Ohm's Law in Weak Electrolytes.* Journal of Chemical Physics, 1934. 2: p. 599.
14. Reiss, K., *Versuche zum Stromleitungsmechanismus in Flüssigkeiten niedriger Dielektrizitätskonstante.* Annalen der Physik, 1936. 420(4): p. 325.
15. Seyed-Yagoobi, J., Atten, P., Bryan, J. E., Feng, Y. and Malraison, B., *Electrohydrodynamically Induced Dielectric Liquid Flow Through Pure Conduction in Point/Plane Geometry - Experimental Study*, in *13th International Conference on Dielectric Liquids*. 1999: Japan: p. 548-551.
16. Plumley, H.J., *Conduction of Electricity by Dielectric Liquids at High Field Strengths.* Physical Review, 1941. 59: p. 200.
17. Melcher, J.R., *Travelling-Wave Induced Electroconvection.* Physics of Fluids, 1966. 9(8): p. 1548-1555.
18. Crowley, J.M., Chang, P., Riley, D. and Chato, J.C., *EHD Induction Pumping in Annuli.* IEEE Transactions on Electrical Insulation, 1985. 20(2).
19. Yeo, L.Y., Chang, H., *Electrowetting on Parallel Line Electrodes.* Physical Review E, 2006. 73; 011605.
20. Cho, G., Kim, D., Kang, S., *Electric field solutions between an emitter tip and a plane extractor in LMIS.* Journal of Physics D: Applied Physics, 1990. 23(1): p. 85-89.
21. Lide, D.R., ed. *CRC Handbook of Chemistry and Physics*. 2003, CRC Press.
22. Pohl, H.A., *Dielectrophoresis the behavior of neutral matter in nonuniform electric fields*. 1978, Cambridge: Cambridge University Press.
23. Green, N.G. and Morgan, H., *Dielectrophoresis of Submicrometer Latex Spheres. 1. Experimental Results* Journal of Physical Chemistry B, 1999. 103: p. 41-50.
24. Basuray, S. Chang, H-C., *Induced dipoles and dielectrophoresis of nanocolloids in electrolytes.* Physical Review E, 2007. 75; 060501.